

**NON-CATALYTIC AND CATALYTIC FAST  
PYROLYSIS OF LIGNOCELLULOSIC BIOMASS  
INTO BIO-OIL OVER ALUMINOSILICATE-  
BASED CATALYSTS**

**TAN YEE LING**

**UNIVERSITI SAINS MALAYSIA**

**2018**

**NON-CATALYTIC AND CATALYTIC FAST PYROLYSIS OF  
LIGNOCELLULOSIC BIOMASS INTO BIO-OIL OVER  
ALUMINOSILICATE-BASED CATALYSTS**

**by**

**TAN YEE LING**

**Thesis submitted in fulfillment of the  
requirements for the degree of  
Doctor of Philosophy**

**November 2018**

## ACKNOWLEDGEMENT

The success and final outcome of this research required a lot of guidance and assistance from many people and I am extremely privileged to have got this all along the completion of my project. All that I have done is only due to such supervision and assistance and I would not forget to thank them.

I respect and thank my supervisor, Prof. Dr. Bassim H. Hameed for providing me an opportunity to join READ group and giving us all support and guidance that made me complete the project duly. I am extremely thankful to him for providing such a nice support and guidance, although he had busy schedule. I am also grateful to my co-supervisor, Prof. Dr. Ahmad Zuhairi Abdullah for his invaluable suggestions. I offer my sincere thanks to Prof. Ir. Dr. Abdul Rahman Mohamed and his student Koh Mei Kee for providing the standard gas for GC-TCD calibration.

I am deeply thankful to Ministry of higher Education (MOHE), Malaysia for the scholarship under the program of MyPhD, MyBrain15. I owe my deep gratitude to all administrative and technical staffs in the School for their valuable help and co-operation. Special thanks to friends in Reaction Engineering and Adsorption (READ) group, especially Dr. Yanna Syamsuddin, Dr. Norhaslinda Nasuha, Dr. Patrick U. Okoye, Dr. Ali Lawan Yaumi, Dr. Kabir Garba, Dr. Waheed Khanday, Fatma Marrackchi and Hamizura who had helped and inspired me throughout my research.

I am always indebted to my family and friends, especially my parents Tan Weng Hock and Choong Cheng Mooi, for supporting and encouraging me to complete my study. Thanks for their understanding my situation and assisting me

throughout my study period so that I can fully concentrate on my research without hesitation.

Sincere appreciations to my colleagues met in USM, there are also many others who have influenced my study positively whose names are not mentioned here. I appreciate all those who had helped at various levels in seeing to the successful completion of this work. The research grant was provided by the Universiti Sains Malaysia, Malaysia, under Research University (RU) TOP-DOWN grant (Project No: 1001/PJKIMIA/8070005). Last but not least, thanks everyone who has directly or indirectly contributed to my research.

*Tan, Yee Ling*

*USM, Penang, November 2018*

## TABLE OF CONTENTS

	<b>Page</b>
<b>ACKNOWLEDGEMENT</b>	ii
<b>TABLE OF CONTENTS</b>	iv
<b>LIST OF TABLES</b>	viii
<b>LIST OF FIGURES</b>	xi
<b>LIST OF PLATES</b>	xvii
<b>LIST OF ABBREVIATIONS</b>	xviii
<b>LIST OF SYMBOLS</b>	xix
<b>ABSTRAK</b>	xx
<b>ABSTRACT</b>	xxii
<b>CHAPTER ONE: INTRODUCTION</b>	
1.1 Biomass as energy and chemical sources	1
1.2 Types of feedstock	3
1.3 Pyrolysis	5
1.4 Problem statements	7
1.5 Research objectives	9
1.6 Scope of study	9
1.7 Thesis organization	10
<b>CHAPTER TWO: LITERATURE REVIEW</b>	
2.1 Introduction	12
2.2 Lignocellulosic biomass	12
2.3 Fast pyrolysis	14
2.4 Catalytic fast pyrolysis	18
2.4.1 Acid catalysts	23
2.4.2 Metal-impregnated catalysts	27
2.5 Effect of reaction parameters on product distribution	35
2.5.1 Effect of biomass particle size	35
2.5.2 Effect of pyrolysis temperature	37
2.5.3 Effect of catalytic bed temperature	40
2.5.4 Effect of catalyst loading	42

2.5.5	Catalyst deactivation and reusability	43
2.6	Reaction kinetic study for thermal and catalytic pyrolysis	45
2.7	Summary	53

### **CHAPTER THREE: MATERIALS AND METHODS**

3.1	Introduction	54
3.2	Experiment flow	54
3.3	Materials and Chemicals	59
3.3.1	Materials	59
3.3.2	Chemicals	59
3.4	Description of equipment	61
3.5	Synthesis of catalysts	64
3.5.1	Synthesis of silica-alumina catalysts	64
3.5.2	Modification of silica-alumina catalyst with calcium and iron	65
3.5.3	Synthesis of industrial waste-derived aluminosilicate catalysts	66
3.6	Characterization of catalysts	66
3.6.1	Surface area and porosity measurement	67
3.6.2	X-ray diffraction (XRD)	67
3.6.3	Scanning Electron Microscopy (SEM) with Energy-dispersive X-ray spectroscopy (EDX)	68
3.6.4	Fourier-transform infrared (FTIR) spectroscopy	68
3.6.5	X-ray fluorescence (XRF)	69
3.6.6	Surface acidity measurement of catalyst by titration method	69
3.6.7	Thermogravimetric analyzer (TGA)	70
3.7	Fast pyrolysis study	70
3.7.1	Thermal fast pyrolysis	71
3.7.2	Catalytic fast pyrolysis	71
3.7.3	Reusability study	72
3.8	Biomass and product analyses	73
3.8.1	Determination of lignocellulosic content of raw biomass	73
3.8.2	Gas chromatography-mass spectrometry (GC-MS)	74
3.8.3	CHNS elemental analyzer	74
3.8.4	Gas chromatography with thermal conductivity detector (GC-	75

	TCD)	
3.8.5	Bomb calorimeter	75
3.8.6	Moisture content determination	76
3.9	Kinetic study of non-catalytic and catalytic decomposition of durian shell	76

## **CHAPTER FOUR: RESULTS AND DISCUSSION**

4.1	Introduction	78
4.2	Thermal fast pyrolysis	78
	4.2.1 Characterization of feedstock	78
	4.2.2 Parameter study of fast pyrolysis	81
4.3	Catalytic fast pyrolysis of durian shell over silica-alumina catalysts	100
	4.3.1 Characterization of silica-alumina catalysts	100
	4.3.2 Catalytic fast pyrolysis of durian shell using silica-alumina catalysts	107
	4.3.3 Concluding remarks for silica-alumina catalysts	124
4.4	Catalytic fast pyrolysis of durian shell over Ca- and Fe-modified silica-alumina catalysts	125
	4.4.1 Characterization of Ca- and Fe-modified silica-alumina catalysts	125
	4.4.2 Catalytic fast pyrolysis of durian shell using modified silica-alumina catalysts	132
	4.4.3 Concluding remarks for Ca- and Fe-modified silica-alumina catalysts	142
4.5	Catalytic fast pyrolysis of durian shell over industrial waste-derived aluminosilicate catalysts	143
	4.5.1 Characterization of industrial waste-derived aluminosilicate catalysts	143
	4.5.2 Catalytic fast pyrolysis of durian shell using industrial waste-derived aluminosilicate catalysts	151
	4.5.3 Concluding remarks for industrial waste-derived aluminosilicate catalysts	162
4.6	Comparison between silica-alumina, modified silica-alumina and	163

	industrial waste-derived aluminosilicate performances in catalytic fast pyrolysis	
4.7	Catalytic fast pyrolysis of karanj shell and rattan over SA-5.1 and AS-EAF catalysts	165
4.7.1	Comparison of SA-5.1 performance on catalytic fast pyrolysis of durian shell, rattan and karanj shell	165
4.7.2	Comparison of AS-EAF performance on catalytic fast pyrolysis of durian shell, rattan and karanj shell	170
4.7.3	Short comparison of SA-5.1 and AS-EAF catalysts' performances on catalytic fast pyrolysis of durian shell, rattan and karanj shell	175
4.8	Catalyst regeneration and reusability	176
4.8.1	Regeneration and reusability of SA-5.1 catalyst	176
4.8.2	Regeneration and reusability of AS-EAF catalyst	183
4.8.3	Short summary on catalyst regeneration and reusability	189
4.9	Kinetic study	190

## **CHAPTER FIVE: CONCLUSION AND RECOMMENDATION**

5.1	Conclusion	199
5.2	Recommendation	201

<b>REFERENCES</b>	202
-------------------	-----

## **APPENDICES**

Appendix A: Calculation of silica/alumina ratio

Appendix B: List of chemical compounds in bio-oils

Appendix C: GC-TCD chromatogram for standard gas

Appendix D: Calculation for Coats-Redfern method

## **LIST OF PUBLICATIONS**



## LIST OF TABLES

		<b>Page</b>
Table 2.1	Summary of product yield distribution in fast pyrolysis of lignocellulosic biomass.	15
Table 2.2	Chemical compositions of bio-oil (Huber et al., 2006).	16
Table 2.3	Reaction mechanisms in catalytic pyrolysis (Liu et al., 2014).	20
Table 2.4	Effect of catalysts on chemical distribution in bio-oil.	33
Table 2.5	Decomposition temperature of biomass components.	37
Table 2.6	Solid-state rate and integral expressions for different reaction models (Khawam and Flanagan, 2006).	48
Table 2.7	Kinetic studies of thermal and catalytic pyrolysis of biomass.	51
Table 3.1	Sources and suppliers of chemicals used for the study.	60
Table 3.2	List of gases used in this study.	61
Table 3.3	List of equipments used in catalyst preparation.	64
Table 4.1	Properties of durian shell, rattan and karanj shell used.	79
Table 4.2	Elemental composition and HHV of pyrolysis products.	99
Table 4.3	BET surface area, pore volume and pore diameter of SA-7.6, SA-5.1 and SA-3.8 catalysts.	102
Table 4.4	EDX analysis of silica-alumina catalysts.	105
Table 4.5	Elemental composition and HHV of durian shell feedstock, non-catalytic and catalytic bio-oil. (Catalytic temperature: 600 °C; catalyst/durian shell ratio = 1:30)	113
Table 4.6	Elemental composition and HHV of catalytic bio-oil produced over SA-5.1 catalyst at different catalytic temperature. (Catalyst/durian shell ratio: 1:30)	119
Table 4.7	Elemental composition and HHV of catalytic bio-oil produced over SA-5.1 catalyst with different catalyst/durian shell ratio. (Catalytic temperature: 500 °C)	124

Table 4.8	BET surface area, pore volume and pore diameter of SA-5.1, 10CaSA and 10FeSA catalysts.	127
Table 4.9	Elemental composition and HHV of catalytic bio-oil produced from durian shell over calcium-modified silica-alumina catalysts. (Catalytic temperature: 500 °C)	137
Table 4.10	Elemental composition and HHV of catalytic bio-oil produced from durian shell over iron-modified silica-alumina catalysts. (Catalytic temperature: 500 °C; catalyst/durian shell ratio: 1:30)	141
Table 4.11	BET surface area, pore volume and pore diameter of SA-5.1, AS-OPA and AS-EAF catalysts.	145
Table 4.12	Elemental composition and HHV of catalytic bio-oil produced from durian shell over industrial waste-derived aluminosilicate catalysts. (Catalytic temperature = 500 °C, catalyst/durian shell ratio = 2:30)	155
Table 4.13	Elemental composition and HHV of catalytic bio-oil produced from durian shell over AS-EAF catalyst at different catalytic temperature. (Catalyst/durian shell ratio = 2:30)	159
Table 4.14	Elemental composition and HHV of catalytic bio-oil produced from durian shell over AS-EAF catalyst at different catalyst/durian shell ratio. (Catalytic temperature: 500 °C)	162
Table 4.15	Comparison of product yield and bio-oil composition in catalytic fast pyrolysis of durian shell.	164
Table 4.16	Elemental composition and HHV of catalytic bio-oil produced from rattan and karanj shell over SA-5.1 catalyst. (Catalytic temperature: 500 °C; catalyst/feedstock ratio: 1:30)	170
Table 4.17	Elemental composition and HHV of catalytic bio-oil produced from rattan and karanj shell over AS-EAF catalyst. (Catalytic temperature: 500 °C; catalyst/feedstock ratio: 2:30)	175
Table 4.18	Elemental composition and HHV of catalytic bio-oil produced from karanj shell with SA-5.1 catalyst for 1 <sup>st</sup> and 5 <sup>th</sup> run (Catalytic temperature: 500 °C, catalyst/karanj shell ratio: 1:30)	180

Table 4.19	Elemental composition and HHV of catalytic bio-oil produced from karanj shell with AS-EAF catalyst for 1 <sup>st</sup> and 5 <sup>th</sup> run (Catalytic temperature = 500 °C, catalyst/karanj shell ratio = 2:30)	186
Table 4.20	Pyrolysis characteristic parameters for thermal and catalytic fast pyrolysis of durian shell.	193
Table 4.21	Kinetic parameters of thermal and catalytic fast pyrolysis of durian shell in Phase II.	195
Table 4.22	Kinetic parameters of thermal and catalytic fast pyrolysis of durian shell in Phase III.	196

## LIST OF FIGURES

		<b>Page</b>
Figure 1.1	Global energy consumption growths from 1992 to 2017 (BP, 2018).	1
Figure 1.2	Fundamental biomass conversion methods and the products (McKendry, 2002).	3
Figure 2.1	Monomer units of (a) cellulose, (b) lignin and (c) hemicellulose (Hansen and Plackett, 2008; Shahzadi et al., 2014).	13
Figure 2.2	The main reactions in pyrolysis mechanism (Wang et al., 2017a).	16
Figure 2.3	Classification of physisorption isotherms.	22
Figure 2.4	Classification of hysteresis loops.	23
Figure 3.1(a)	Flow chart of non-catalytic fast pyrolysis.	56
Figure 3.1(b)	Flow chart of catalytic fast pyrolysis of durian shell over silica-alumina and calcium- or iron-modified silica-alumina catalysts.	57
Figure 3.1(c)	Flow chart of catalytic fast pyrolysis over industrial waste-derived aluminosilicate catalysts, catalyst reusability study and kinetic study.	58
Figure 3.2	Schematic diagram of catalytic fast pyrolysis reactor.	62
Figure 4.1	Effect of particle size on product yield (a) char, (b) bio-oil and (c) gas. (Reaction condition: Pyrolysis temperature = 550 °C, mass of feedstock = 3 g)	82
Figure 4.2	Effect of pyrolysis temperature on product yield produced from (a) durian shell, (b) rattan and (c) karanj shell. (Reaction condition: size of durian shell = 1-2 mm, size of rattan and karanj shell = 0.5-1 mm, mass of feedstock = 3 g)	85
Figure 4.3	Water content of bio-oil produced from fast pyrolysis of durian shell, rattan and karanj shell. (Reaction condition: size of durian shell = 1-2 mm, size of rattan and karanj shell = 0.5-1 mm, mass of feedstock = 3 g)	88

Figure 4.4	Effect of pyrolysis temperature on composition of gaseous product obtained from fast pyrolysis of (a) durian shell, (b) rattan and (c) karanj shell. (Reaction condition: size of durian shell = 1-2 mm, size of rattan and karanj shell = 0.5-1 mm, mass of feedstock = 3 g)	89
Figure 4.5	Detailed species distribution of chemicals in bio-oil obtained from fast pyrolysis of durian shell at different temperature. (Reaction condition: Size of durian shell = 1-2 mm, mass of durian shell = 3 g)	92
Figure 4.6	Detailed species distribution of chemicals in bio-oil obtained from fast pyrolysis of rattan at different temperature. (Reaction condition: Size of rattan = 0.5-1 mm, mass of rattan = 3 g)	94
Figure 4.7	Detailed species distribution of chemicals in bio-oil obtained from fast pyrolysis of karanj shell at different temperature. (Reaction condition: Size of karanj shell = 0.5-1 mm, mass of karanj shell = 3 g)	96
Figure 4.8	(a) N <sub>2</sub> adsorption-desorption isotherms and (b) pore size distribution of silica-alumina catalysts.	101
Figure 4.9	XRD pattern of SA-5.1 catalyst.	103
Figure 4.10	SEM images of SA-7.6 at magnification of (a) 10000× and (b) 30000×, SA-5.1 at magnification of (c) 10000× and (d) 30000×, SA-3.8 at magnification of (e) 10000× and (f) 30000×.	105
Figure 4.11	FTIR spectra of (a) SA-7.6, SA-5.1 and (c) SA-3.8 catalysts.	106
Figure 4.12	Effect of silica/alumina ratio of catalyst on (a) product yield and (b) gas composition. (Reaction condition: Mass of durian shell = 3 g, catalyst/durian shell ratio = 1:30, catalytic bed temperature = 600 °C)	108
Figure 4.13	Detailed species distribution of chemicals in bio-oil obtained from catalytic fast pyrolysis of durian shell with silica-alumina catalysts. (Reaction condition: Mass of durian shell = 3 g, catalyst/durian shell ratio = 1:30, catalytic bed temperature = 600 °C)	111
Figure 4.14	Effect of catalytic temperature on (a) product yield and (b) gas composition. (Reaction condition: Mass of durian shell = 3 g, catalyst/durian shell ratio = 1:30)	115

Figure 4.15	Detailed species distribution of chemicals in bio-oil obtained from catalytic fast pyrolysis of durian shell with SA-5.1 catalyst at different catalytic temperature. (Reaction condition: Mass of durian shell = 3 g, catalyst/durian shell ratio = 1:30)	117
Figure 4.16	Effect of catalytic/durian shell ratio on (a) product yield and (b) gas composition. (Reaction condition: Mass of durian shell = 3 g, catalytic temperature = 500 °C)	120
Figure 4.17	Detailed species distribution of chemicals in bio-oil obtained from catalytic fast pyrolysis of durian shell with SA-5.1 catalyst at different catalytic/durian shell ratio. (Reaction condition: Mass of durian shell = 3 g, catalytic temperature = 500 °C)	122
Figure 4.18	(a) N <sub>2</sub> adsorption-desorption isotherms and (b) pore size distribution of 10CaSA and 10FeSA catalysts.	126
Figure 4.19	XRD patterns of (a) 10FeSA, (b) 10CaSA and (c) SA-5.1 catalysts.	128
Figure 4.20	SEM images of 10CaSA at magnification of (a) 10000× and (b) 30000×, and 10FeSA at magnification of (c) 10000× and (d) 30000×.	129
Figure 4.21	EDX analysis result of (a) 10CaSA and (b) 10FeSA catalysts.	130
Figure 4.22	FTIR spectra of (a) 10CaSA, (b) 15CaSA, (c) 20CaSA, (d) 2FeSA, (e) 6FeSA and (f) 10FeSA catalysts.	131
Figure 4.23	Effect of calcium content on (a) product yield and (b) gas composition. (Reaction condition: Mass of durian shell = 3 g, catalytic temperature = 500 °C, catalyst/durian shell ratio = 1:30)	133
Figure 4.24	Detailed species distribution of chemicals in bio-oil obtained from catalytic fast pyrolysis of durian shell with calcium-modified silica-alumina catalysts. (Reaction condition: Mass of durian shell = 3 g, catalytic temperature = 500 °C, catalyst/durian shell ratio = 1:30)	135
Figure 4.25	Effect of iron content on (a) product yield and (b) gas composition. (Reaction condition: Mass of durian shell = 3 g, catalytic temperature = 500 °C, catalyst/durian shell ratio = 1:30)	138

Figure 4.26	Detailed species distribution of chemicals in bio-oil obtained from catalytic fast pyrolysis of durian shell with iron-modified silica-alumina catalysts. (Reaction condition: Mass of durian shell = 3 g, catalytic temperature = 500 °C, catalyst/durian shell ratio = 1:30)	140
Figure 4.27	(a) N <sub>2</sub> adsorption-desorption isotherms and (b) pore size distribution of AS-OPA and AS-EAF catalysts.	144
Figure 4.28	XRD patterns of (a) AS-OPA and (b) AS-EAF catalysts.	146
Figure 4.29	SEM images of AS-OPA at magnification of (a) 5000× and (b) 10000×, and AS-EAF at magnification of (c) 5000× and (d) 10000×.	148
Figure 4.30	EDX analysis result of (a) AS-OPA and (b) AS-EAF catalysts.	149
Figure 4.31	FTIR spectra of (a) AS-OPA and (b) AS-EAF catalysts.	150
Figure 4.32	Effect of AS-OPA and AS-EAF catalysts on (a) product yield and (b) gas composition. (Reaction condition: Mass of durian shell = 3 g, catalytic temperature = 500 °C, catalyst/durian shell ratio = 2:30)	152
Figure 4.33	Detailed species distribution of chemicals in bio-oil obtained from catalytic fast pyrolysis of durian shell with SA-5.1, AS-OPA and AS-EAF catalysts. (Reaction condition: Mass of durian shell = 3 g, catalytic temperature = 500 °C, catalyst/durian shell ratio = 2:30)	153
Figure 4.34	Effect of catalytic temperature on (a) product yield and (b) gas composition. (Reaction condition: Mass of durian shell = 3 g, catalyst/durian shell ratio = 2:30)	156
Figure 4.35	Detailed species distribution of chemicals in bio-oil obtained from catalytic fast pyrolysis of durian shell with AS-EAF catalyst at different catalytic temperature. (Reaction condition: Mass of durian shell = 3 g, catalyst/durian shell ratio = 2:30)	157
Figure 4.36	Effect of catalyst/durian shell ratio on (a) product yield and (b) gas composition. (Reaction condition: Mass of durian shell = 3 g, catalyst/durian shell ratio = 2:30)	160
Figure 4.37	Detailed species distribution of chemicals in bio-oil obtained from catalytic fast pyrolysis of durian shell with AS-EAF catalyst at different catalyst/durian shell ratio. (Reaction condition: Mass of durian shell = 3 g, catalytic temperature = 500 °C)	161

Figure 4.38	(a) Product yield and (b) gas composition obtained by thermal and catalytic fast pyrolysis over SA-5.1 catalyst using durian shell (DS), rattan and karanj shell (KS). (Reaction condition: Mass of feedstock = 3 g, catalytic temperature = 500 °C, catalyst/feedstock ratio = 1:30)	166
Figure 4.39	Detailed species distribution of chemicals in bio-oil obtained from thermal and catalytic fast pyrolysis of durian shell (DS), rattan and karanj shell (KS) with SA-5.1 catalyst. (Reaction condition: Mass of feedstock = 3 g, catalytic temperature = 500 °C, catalyst/feedstock ratio = 1:30)	168
Figure 4.40	(a) Product yield and (b) gas composition obtained by thermal and catalytic fast pyrolysis over AS-EAF catalyst using durian shell (DS), rattan and karanj shell (KS). (Reaction condition: Mass of feedstock = 3 g, catalytic temperature = 500 °C, catalyst/feedstock ratio = 2:30)	171
Figure 4.41	Detailed species distribution of chemicals in bio-oil obtained from thermal and catalytic fast pyrolysis of durian shell, rattan and karanj shell with AS-EAF catalyst. (Reaction condition: Mass of feedstock = 3 g, catalytic temperature = 500 °C, catalyst/feedstock ratio = 2:30)	173
Figure 4.42	Effect of catalyst reusability of SA-5.1 on (a) product yield and (b) gas composition. (Reaction condition: Mass of karanj shell = 3 g, catalytic temperature = 500 °C, catalyst/karanj shell ratio = 1:30)	177
Figure 4.43	Detailed species distribution of chemicals in bio-oil obtained from catalytic fast pyrolysis of karanj shell with SA-5.1 catalyst for 1 <sup>st</sup> , 3 <sup>rd</sup> and 5 <sup>th</sup> run. (Reaction condition: Mass of karanj shell = 3 g, catalytic temperature = 500 °C, catalyst/karanj shell ratio = 1:30)	179
Figure 4.44	FTIR spectra of (a) fresh and (b) used SA-5.1 catalyst after 5 cycles.	181
Figure 4.45	SEM images of (a) fresh SA-5.1 catalyst, (b) spent SA-5.1 catalyst and (c) EDX analysis of spent SA-5.1 catalyst after five cycles.	182
Figure 4.46	Effect of catalyst reusability of AS-EAF on (a) product yield and (b) gas composition. (Reaction condition: Mass of karanj shell = 3 g, catalytic temperature = 500 °C, catalyst/karanj shell ratio = 2:30)	184



Figure 4.47	Detailed species distribution of chemicals in bio-oil obtained from catalytic fast pyrolysis of karanj shell with AS-EAF catalyst for 1 <sup>st</sup> , 3 <sup>rd</sup> and 5 <sup>th</sup> run. (Reaction condition: Mass of karanj shell = 3 g, catalytic temperature = 500 °C, catalyst/karanj shell ratio = 2:30)	185
Figure 4.48	FTIR spectra of (a) fresh AS-EAF catalyst and (b) used AS-EAF catalyst after 5 cycles.	187
Figure 4.49	SEM images of (a) fresh AS-EAF, (b) spent AS-EAF and (c) EDX analysis of spent AS-EAF after five cycles.	188
Figure 4.50	(a) Thermogravimetric and (b) derivative thermogravimetric curves for the pyrolysis of durian shell (DS), durian shell with SA-5.1 catalyst and durian shell with AS-EAF catalyst at heating rate of 100 °C/min.	191

## LIST OF PLATES

	<b>Page</b>
Plate 3.1      Image of catalytic fast pyrolysis reactor.	63

## LIST OF ABBREVIATIONS

SVR	Surface area-to-volume ratio
BTX	Benzene, toluene and xylene
TGA	Thermogravimetric analysis
DTG	Differential thermal gravimetric
EAF	Electric arc furnace
OPA	Oil palm ash
XRF	X-ray fluorescence
SEM	Scanning electron microscopy
EDX	Energy dispersive X-ray spectroscopy
FTIR	Fourier-transform infrared spectroscopy
BET	Brunauer–Emmett–Teller
XRD	X-ray powder diffraction
GC-MS	Gas chromatography–mass spectrometry
TEOS	Tetraethyl orthosilicate
CTAB	Hexadecyltrimethylammonium bromide
BJH	Barrett–Joyner–Halenda
ICSD	International Crystal Structure Database
GC-TCD	Gas Chromatography-Thermal Conductivity Detector

## LIST OF SYMBOLS

<b>Symbol</b>	<b>Description</b>	<b>Unit</b>
k	Rate constant	s <sup>-1</sup> or min <sup>-1</sup>
A	Pre-exponential factor	s <sup>-1</sup> or min <sup>-1</sup>
E <sub>a</sub>	Apparent activation energy	kJ/mol
R	Universal gas constant	J/K mol <sup>-1</sup>
T	Absolute temperature	K
α	Conversion	-
t	Process time	min
D	Comprehensive devolatilization index	% <sup>2</sup> °C <sup>-3</sup> min <sup>-2</sup>
C <sub>A</sub>	Acid concentration	μmol/g
C <sub>B</sub>	Base concentration	μmol/g
A <sub>exp</sub>	Experimental peak area of a gas	25 μv * s
$\bar{A}_{std}$	Average peak area of the gas in standard gas	25 μv*s
-R <sub>p</sub>	Maximum pyrolysis rate	% min <sup>-1</sup>
-R <sub>v</sub>	Average pyrolysis rate	% min <sup>-1</sup>
T <sub>p</sub>	Temperature corresponded to the local maximum value in DTG curve	°C
ΔT <sub>1/2</sub>	Temperature width at half value of R <sub>p</sub>	°C

**PIROLISIS PANTAS TANPA MANGKIN DAN BERMANGKIN BIOJISIM  
LIGNOSELULOSA KEPADA BIOMINYAK DI ATAS MANGKIN  
BERASASKAN ALUMINOSILIKAT**

**ABSTRAK**

Susutan sumber fosil dan peningkatan motivasi untuk membangunkan bahan api cecair dan bahan kimia yang boleh diperbaharui telah menimbulkan minat dalam kajian penukaran biojisim. Kajian ini bertujuan untuk mengkaji hasil dan kualiti produk yang diperolehi daripada pirolisis pantas haba dan bermangkin bagi kulit durian, rotan dan kulit karanj dalam reaktor lapisan tetap dua peringkat oleh pemangkin silika-alumina dengan nisbah silika/alumina yang berbeza, silika-alumina yang diubahsuai dengan kalsium atau besi, dan pemangkin aluminosilikat yang berasal dari sisa industri. Kesan saiz zarah (sehingga 5 mm) dan suhu pirolisis (250-650 °C) diselidiki dalam pirolisis pantas haba manakala kesan suhu pemangkinan, nisbah pemangkin/stok suapan, jenis stok suapan, dan penjanaan semula pemangkin ditentukan dalam pirolisis pantas bermangkin. Suhu terbaik untuk pengeluaran cecair untuk kulit durian, rotan dan kulit karanj masing-masing ialah 650 °C, 550 °C dan 550 °C. Pemangkin silika-alumina dengan ciri-ciri mikroliang telah disintesis dengan menggunakan kaedah pemendakan bersama. Biominyak yang dihasilkan daripada kulit durian ke atas pemangkin silika-alumina dengan nisbah silika/alumina 5.1 (SA-5.1) pada 600 °C mempunyai tahap penyahoksigenan 93.61% dengan kandungan aromatik 75.45%. Penambahan kalsium megurangkan pemendapan kok pada SA-5.1 manakala besi mempromosikan hasil aromatik dan hidrokarbon. Pemangkin yang dihasilkan oleh arka elektrik jermang relau (AS-EAF) menghasilkan 50.21 wt% biominyak dengan tahap penyahoksigenan 85.49% dan kandungan hidrokarbon 72.82% pada 500 °C. SA-5.1 mempromosikan pembentukan ester dalam pirolisis

pantas bermangkin rotan dan pembentukan aromatik dan hidrokarbon dalam pirolisis pantas bermangkin kulit karanj. AS-EAF mempromosikan hasil ester dan hidrokarbon dalam bi minyak yang dihasilkan daripada rotan, dan hasil aromatik dalam bi minyak yang dihasilkan daripada kulit karanj. Kok yang dimendap di SA-5.1 dan AS-EAF dalam pirolisis pantas bermangkin kulit durian masing-masing adalah 12.68 wt% dan 1.95 wt%. SA-5.1 mempunyai prestasi yang lebih baik selepas penjaan semula dalam pirolisis pantas bermangkin kulit karanj, di mana tahap penyahoksigenan meningkat daripada 35.15% kepada 57.13% dan pemendapan kok menurun daripada 15.71% kepada 11.42%. Walaupun tahap penyahoksigenan bi minyak yang dihasilkan daripada kulit karanj ke atas AS-EAF menurun selepas lima kitaran, pemendapan kok adalah 3.91 wt% selepas digunakan, iaitu lebih rendah daripada SA-5.1. Parameter kinetik dikira menggunakan kaedah Coats-Redfern. Model tindak balas pirolisis haba dan bermangkin kulit durian di Fasa II disumbangkan untuk model penyebaran satu arah manakala Fasa III pirolisis haba dan bermangkin mengikuti model tindak balas tertib kedua atau ketiga. Pirolisis bermangkin dengan SA-5.1 mempamerkan tenaga pengaktifan yang lebih rendah sebanyak 115.55 kJ/mol berbanding dengan pirolisis haba dengan tenaga pengaktifan 170.84 kJ/mol dalam Fasa III, menunjukkan SA-5.1 menggalakkan penguraian lignin.

**NON-CATALYTIC AND CATALYTIC FAST PYROLYSIS OF  
LIGNOCELLULOSIC BIOMASS INTO BIO-OIL OVER  
ALUMINOSILICATE-BASED CATALYSTS**

**ABSTRACT**

Depletion of fossil resources and increasing motivation to develop renewable liquid fuels and chemicals have generated interest in the study of biomass conversion. This study aims to study the product yield and quality obtained from thermal and catalytic fast pyrolysis of durian shell, rattan and karanj shell in two-stage fixed-bed reactor over silica-alumina catalyst with different silica/alumina ratios, calcium- or iron-modified silica-alumina, and industrial waste-derived aluminosilicate catalysts. Effects of particle size (up to 5 mm) and pyrolysis temperature (250-650 °C) were investigated in thermal fast pyrolysis while the effects of catalytic temperature, catalyst/feedstock ratio, types of feedstock, and catalyst regeneration were determined in catalytic fast pyrolysis. The best temperature for liquid production for durian shell, rattan and karanj shell was 650 °C, 550 °C and 550 °C, respectively. Silica-alumina catalyst with microporous characteristic was synthesized using co-precipitation method. The bio-oil produced from durian shell over silica-alumina catalyst with silica/alumina ratio of 5.1 (SA-5.1) at 600 °C has deoxygenation degree of 93.61% with 75.45% aromatics content. The addition of calcium reduced coke deposition on SA-5.1 while iron promoted the yield of aromatics and hydrocarbons. Electric-arc-furnace-slag-derived catalyst (AS-EAF) produced 50.21 wt% bio-oil with deoxygenation degree of 85.49% and 72.82% hydrocarbons content at 500 °C. SA-5.1 promoted the formation of esters in catalytic fast pyrolysis of rattan and the formation of aromatics and hydrocarbons in catalytic fast pyrolysis of karanj shell. AS-EAF promoted the yield of esters and hydrocarbon in bio-oil produced from

rattan, and the yield of aromatics in bio-oil produced from karanj shell. The coke deposited on SA-5.1 and AS-EAF in catalytic fast pyrolysis of durian shell is 12.68 wt% and 1.95 wt%, respectively. SA-5.1 has better performance after regeneration in catalytic fast pyrolysis of karanj shell at 500 °C, which the deoxygenation degree increased from 35.15% to 57.13% and the coke deposition decreased from 15.71 wt% to 11.42 wt%. Although deoxygenation degree of bio-oil produced from karanj shell over AS-EAF reduced after five cycles, the coke deposition was 3.91 wt% after used, which is lower than that of SA-5.1. The kinetic parameters were calculated using Coats-Redfern method. The reaction models of thermal and catalytic pyrolysis of durian shell in Phase II are accounted for one-way diffusion model while the Phase III of thermal and catalytic pyrolysis follows second or third-order reaction models. Catalytic pyrolysis with SA-5.1 exhibited lower activation energy of 115.55 kJ/mol than thermal pyrolysis with activation energy of 170.84 kJ/mol in Phase III, indicates SA-5.1 promoted lignin decomposition.



# CHAPTER ONE

## INTRODUCTION

### 1.1 Biomass as energy and chemical sources

Along with socio-economic development and population increases, the consumption of fossil fuel, especially crude oil, as energy and chemical sources is also increasing. The International Energy Agency (IEA) proposed that the world energy demand in year 2020 will be 50% higher than the energy demand in year 2005, and this value will be three times higher in year 2060 (Tolmac et al., 2014). BP (2018) found that the global oil consumption in 2017 was 98 million barrels per day while the natural gas consumption was 3.67 billion cubic meters in 2017, as shown in Figure 1.1.

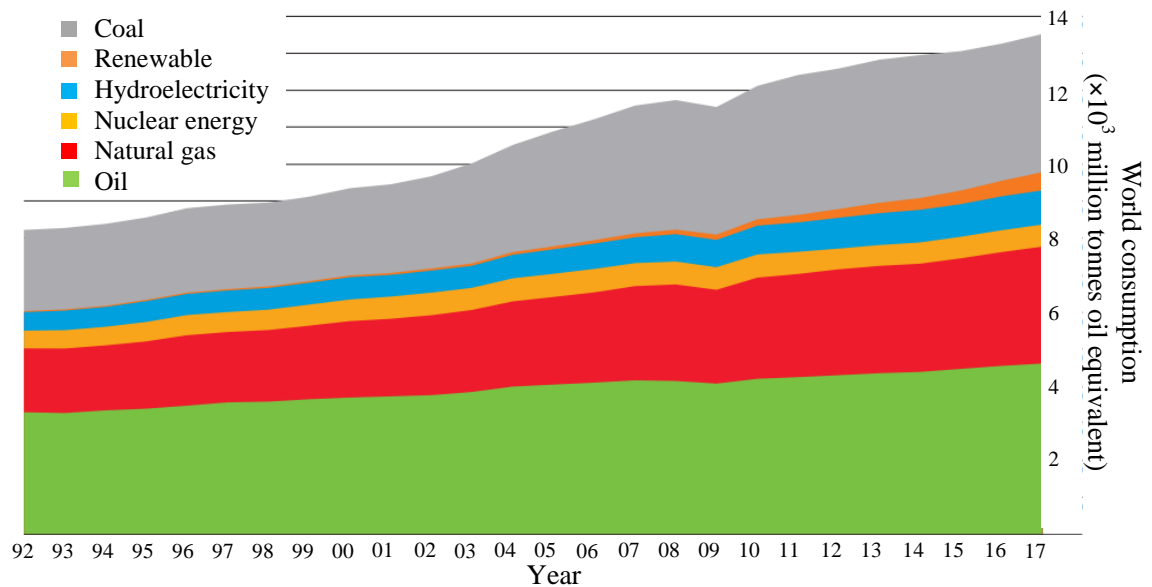


Figure 1.1 Global energy consumption grows from 1992 to 2017 (BP, 2018).

The massive usage of fossil fuel leads to global climate changes and atmospheric pollutions. The combustion of fossil fuels contributes to the formation of greenhouse gases such as carbon dioxide, sulphur oxide and nitrous oxide. The

greenhouse gases will trap heat in the atmosphere and lead to global warming. Besides that, the fluctuating price and availability of fossil fuel are also the major challenges of the continuous economy growth. The negative impacts of using fossil fuel increase the interest of scientists in looking for alternative energy and chemical sources that are sustainable and environmental friendly (Mohan et al., 2006).

Biomass energy is one of the most popular clean energy being used from ancient time which is cheap and abundantly available. Zero carbon emission can be achieved in biomass energy because the carbon dioxide released can be recycled in photosynthesis. Renewable biomass can be converted into fuels and chemicals with suitable conversion technologies such as physicochemical, biochemical and thermochemical processes (Gollakota et al., 2016). Physicochemical conversion involves the biomass conversion through physical and chemical process at ambient temperature and pressure such as the production of biodiesel by transesterification. Biochemical conversion requires the use of bacteria or microorganisms to decompose the biomass such as the formation of bioethanol from corn or sugarcane by fermentation and the production of methane gas by anaerobic digestion. Biochemical conversion of biomass has the advantages of being environmental friendly and requiring no extra energy required but it is an expensive and time-consuming process. Thus, a considerable amount of literature has been published on thermochemical conversion of lignocellulosic biomass, such as the combustion, gasification, pyrolysis (Figure 1.2). These reactions are usually carried out under heating and some of the processes are done under pressure.

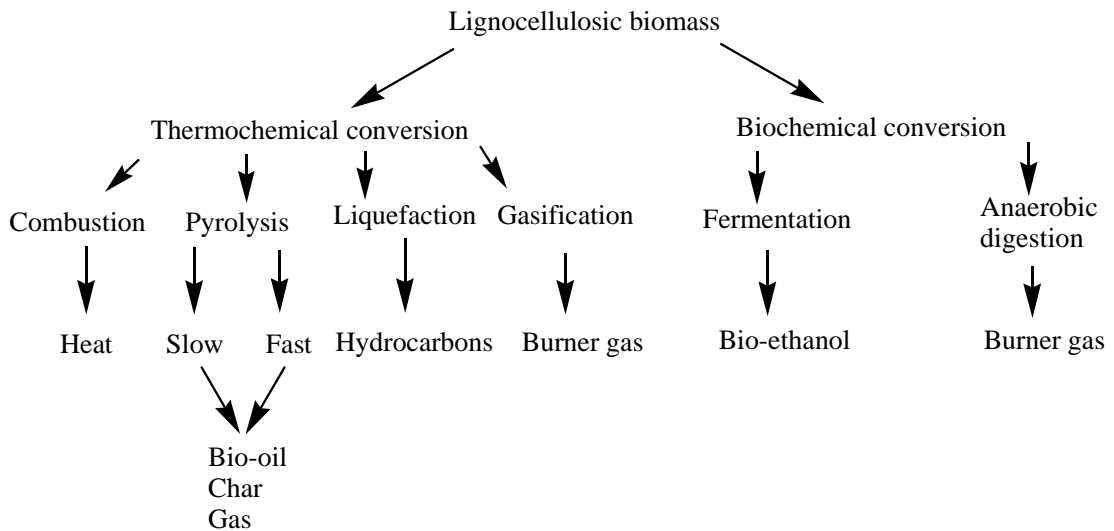


Figure 1.2 Fundamental biomass conversion methods and the products (McKendry, 2002).

Combustion is carried out with sufficient oxygen supply while the products are heat and flame. Gasification and pyrolysis involve the decomposition of biomass with partial or no oxygen supplied. The product of gasification is combustible gas such as carbon monoxide and hydrogen while the pyrolysis products are bio-char, bio-oil and non-condensable permanent gases. Liquefaction involves the conversion of biomass into stable liquid hydrocarbons in a pressure vessel at relatively low temperature (280-370 °C) and high pressure (10-25 MPa) (Dimitriadis and Bezergianni, 2017). The process can be selected by considering the desired products and reaction conditions.

## 1.2 Types of feedstock

The composition of pyrolysis oil is affected by the types of feedstock and process condition, e.g. feedstock with high lignin produces bio-oil with high phenolic content while feedstock rich in holocellulose (cellulose and hemicellulose) tends to produce bio-oil with more furan-derived chemicals such as organic acids and carbonyls (Huber et al., 2006). In order to determine the effect of biomass

composition on product yield and bio-oil composition, durian shell that rich in cellulose, rattan that rich in hemicellulose and karanj shell that rich in lignin content were selected as feedstock in this study.

**(a) Durian shell**

Durian (*Durrio zabethinus Linn*), a member of the Bombaceae family, is one of the most popular tree in Southeast Asia, especially in Malaysia, Indonesia, Thailand, and the Philippines (Amid and Mirhosseini, 2012). In Malaysia, the production of durian fruit is approximately 320,164 MT in 2013, as reported by Manshor et al. (2014). Non-edible durian parts such as shell and seeds (70%-85% of the whole fruit) are discarded as wastes, thereby causing pollution if not disposed properly. The improper disposal of durian wastes may cause respiratory diseases, pungent smell, and water pollution (Prakongkep et al., 2014). Durian shell consists of 60.5% cellulose, 13.1% hemicellulose, and 15.45% lignin (Masrol et al., 2015). This high cellulosic composition makes it a highly attractive feedstock to be used in pyrolysis study.

**(b) Rattan**

Rattan, a member of the Palmae/Arecaceae family, is one of the commonly used materials in furniture manufacturing, especially in Southeast Asia. There are about 600 different rattan species belonging to 13 genera in the world, while there are 106 species are available in Malaysia (Dransfield, 1979). During the furniture making process, over 30% of the rattan is disposed as wastes (Olorunnisola, 2005). The improper disposal of rattan wastes such as open burning and illegal dumping may cause environment pollution (Islam et al., 2017). Rattan cane consists of ~50%

cellulose, ~25% hemicellulose, and ~20% lignin (Ma et al., 2017a). The high polysaccharides content makes it a potential feedstock to produce pyrolysis oil.

**(c) Karanj shell**

Karanj (*Pongamia pinnata*), a member of Fabaceae family, is a popular feedstock to produce non-edible oil as bio-diesel precursor. It can be easily found in tropical and sub-tropical countries such as Southeast Asia and India. Karanj is a flat and elliptical fruit that consists of fruit shell and seed. The seeds are used for oil extraction and the fruit shells are usually disposed as waste. Karanj shell consists of 59.5% cellulose and hemicellulose and 40.5% lignin (Prasad et al., 2015). It has high lignin content that makes it a potential feedstock to produce bio-oil with high aromatic content.

### **1.3 Pyrolysis**

Pyrolysis is a promising thermochemical technology that involves rupture of organic chemical bonds with no or partial oxygen supply to produce light gases, tar and char (Bridgwater et al., 2002). Permanent gases such as carbon oxides, hydrogen and light hydrocarbon gases are released during the pyrolysis process while the tar can be further converted into light gases, char and soot through secondary reactions (Migliavacca et al., 2005). Bio-char can be a potential solid fuel and the pyrolysis gas can be used to produce syngas through water-gas shift reaction.

Pyrolysis has one advantage that the reaction condition can be adjusted according to desired product. For example, slow pyrolysis with vapour residence time from 5 min to 30 min favours the formation of bio-char while fast pyrolysis with short residence time that less than 5 seconds favoured the production of bio-oil (Bridgwater, 2012; Liu et al., 2014). The essential features of fast pyrolysis was

summarized by Bridgwater (2012), which are (a) the high heating rate (~1000 K/s) and heat transfer rate across biomass particles, (b) intermediate temperature around 500 °C to maximize liquid production, (c) short vapour residence time to minimize secondary reactions, (d) rapid removal of solid char to avoid secondary cracking of pyrolysis vapour, and (e) the rapid quenching of pyrolysis vapour into bio-oil.

Bio-oil is formed by immediate quenching of the pyrolysis vapor and composed of different condensable chemicals, mainly oxygenated compounds. The presence of oxygenated compounds leads to the poor fuel characteristics of unprocessed bio-oil such as corrosive, lower calorific value, higher viscosity, thermal instability and it might be non-homogeneous (Gollakota et al., 2016). The applications of upgraded bio-oil were reviewed by Gollakota et al. (2016), such as combustion fuel, power generation, production of resins and chemicals, production of anhydrosugars and wood preservatives. Different upgrading techniques were investigated such as hydrotreatment techniques, catalytic cracking, steam reforming and esterification. Hydrotreatment techniques such as hydrodeoxygenation, hydrodenitrogenation, hydrodesulphurization, hydrodemetallization and hydrogenation are the most effective way to upgrade the bio-oil but it is undesirable because hydrogen is expensive and high pressure is required (Mettler et al., 2012). Thus, hydrogen-free direct approaches are investigated and developed.

Catalytic cracking and deoxygenation involve the contact of catalyst with pyrolysis vapour to remove oxygen as water, carbon monoxide and carbon dioxide. Kabir and Hameed (2017) classified the catalysts used in catalytic pyrolysis into two groups: acid and base catalysts. Solid acids are the main catalysts used in catalytic cracking of bio-oil due to the excellent cracking performance and suitable pore structure. Fan et al. (2017) suggested that the product yield distribution is mainly

affected by pore size while the chemical composition of bio-oil is influenced by acid strength of catalyst. Yu et al. (2012) suggested the “effective pore size” of catalyst increased at higher temperature and this affects the product selectivity. Besides that, Mihalcik et al. (2011) found that the external acid sites mainly work on cracking of large molecules while the internal acid sites focus on aromatization and produce more aromatic compounds. Thus, the tuning of catalyst properties is crucial for the product yield and bio-oil composition. Besides that, the effects of catalyst acidity and pore structure on coke deposition were investigated to improve catalyst reusability (Mukarakate et al., 2014). Although zeolite is effective at oxygen removal due to it is highly acidic and its microporous structure, the small pore size also hinders the diffusion of bulk molecules and thus the external pores are blocked and leads to catalyst deactivation (Xu et al., 2017). In order to overcome the problem of catalyst deactivation due to coke formation, the application of base catalyst in catalytic pyrolysis is investigated. Base catalysts are potential in breaking large molecules with lower poisoning of active sites because of the continuous removal of water vapour and carbon dioxide, and also the larger pore size for molecules diffusion.

#### **1.4 Problem statements**

Fast pyrolysis is favourable in biomass-to-liquid conversion because the long vapour residence time of slow pyrolysis leads to secondary reactions and lower liquid yield with poorer product properties (Campanella and Harold, 2012). Fast pyrolysis of different lignocellulosic biomass was widely reported, especially the decomposition mechanisms of individual biomass components. Fundamental understanding of thermal decomposition mechanisms of biomass is important in controlling the chemical composition of end-product. The chemical composition of biomass will affect the quality of products, especially for bio-oil. Most studies

reported the chemical composition obtained from decomposition of individual biomass components (cellulose, hemicellulose and lignin) but the relation between real biomass with different compositions and product composition is not well established. The decomposition of biomass can be investigated by studying the gas composition obtained across a range of temperature. However, the utilization of crude bio-oil is limited due to the vast chemical compositions of bio-oil which consisted of carboxylic acids, alcohol, carbonyls, esters, furan derivatives, nitrogen-containing compounds, pyran derivatives, anhydrosugars, aromatic and aliphatic hydrocarbons. Thus, catalytic upgrading of bio-oil is crucial.

In current stage, most of the studies reported the catalytic fast pyrolysis through in-situ method, which involves the mixing of catalyst and feedstock. However, the in-situ method is not suitable for the regeneration study because it is very hard to separate the used catalyst from the solid product. Thus, ex-situ catalytic fast pyrolysis that involves the formation of pyrolysis vapour and upgrading in single reactor without direct contact between catalyst and feedstock is a good alternative method. The major challenge in catalytic fast pyrolysis is to avoid rapid catalyst deactivation due to the formation of undesired coke. The deoxygenation performance and aromatic production of ZSM-5 are well investigated but the amount of coke deposited is usually high. Thus, aluminosilicate catalysts with different pore size are synthesized and used in the catalytic pyrolysis process. The textural and porous properties are modified by tuning the silica/alumina ratio or adding metal oxide to enhance the product yield and selectivity while the catalyst lifetime is maximized.

Kinetic study is important to predict the product yield and optimize process conditions. However, the heating rates reported in literatures are usually lower than 50 °C/min due to the limitation of commercial instrument. Thus, kinetic study at



higher heating rate (higher than 100 °C/min) is needed to understand the fast pyrolysis behaviour. The decomposition behaviour of biomass with and without catalysts can be compared by fitting to the model-fitting Coats-Redfern model.

## **1.5 Research objectives**

The objectives of this study are to:

- i. Investigate the effect of biomass composition, particle size and temperature on product yield and composition in fast pyrolysis of durian shell, rattan and karanj shell.
- ii. Prepare and characterize aluminosilicate catalysts with different acid-base and textural properties.
- iii. Investigate the catalytic performance of the as-prepared catalysts in catalytic fast pyrolysis of different feedstock under different operating parameters.
- iv. Evaluate the kinetic parameters of fast pyrolysis of durian shell with and without silica-alumina and industrial waste-derived aluminosilicate catalysts.

## **1.6 Scope of study**

The scope of this study covers the fast pyrolysis of three lignocellulosic biomass: durian shell, rattan and karanj shell. The selection of biomass is based on the maximum liquid yield  $\geq 40$  wt% to avoid further reduction of liquid yield in catalytic reaction, and the chemical composition is not important as further upgrading will be done. The reaction parameters such as effect of particle size and temperature are evaluated. The product yield, bio-oil composition and gas composition obtained from different operating conditions are compared to determine best reaction condition for each biomass.

Different aluminosilicate catalysts are developed, characterized and used in the catalytic fast pyrolysis of different types of biomass. Catalysts were prepared using co-precipitation and hydrothermal method. Different preparation parameters such as silica-to-alumina ratio (3.8 to 7.6), metal loading (calcium: 10-20%; iron: 2 to 10%) and industrial waste (oil palm ash and electric arc furnace slag) are employed to determine the suitable catalyst. The as-prepared catalysts are characterized using surface area analyzer, scanning electron microscope with energy dispersive X-ray (SEM/EDX), Fourier-transform infrared spectroscopy (FTIR), Boehm titration and X-ray diffractometer (XRD).

The main idea of catalytic fast pyrolysis is to develop a catalyst that is efficient in aromatic or hydrocarbon production, low coke deposition, and can be used for five cycles after regeneration. The operating conditions such as catalytic temperature (400 °C to 600 °C) and catalyst/feedstock ratio (1:30 to 3:30) are studied to establish the best conditions for catalytic fast pyrolysis and tested with different types of feedstock. The pyrolysis behaviours and kinetic parameters of durian shell decomposition with and without catalysts are determined using thermogravimetric analyzer.

## **1.7 Thesis organization**

This thesis is organized into five chapters.

- Chapter one summarizes the impact of fossil fuel application and the potential of pyrolysis to be used to produce clean fuel and environmental friendly chemicals. The problem statement, research objectives, research scope and thesis organization are discussed in this chapter.

- Chapter two reviews the previous pyrolysis studies of lignocellulosic biomass, catalysts (aluminosilicate catalysts and metal-impregnated catalysts) and effects of reaction parameters (particle size, pyrolysis temperature, catalytic temperature, catalyst loading, and catalyst deactivation and reusability) on product yield distribution. Also, the kinetic studies of biomass decomposition by Coats-Redfern calculation are reviewed.
- Chapter three presents the experimental flow and reactor description. The materials, chemicals and equipments used in this study are listed. The preparation of catalysts, catalyst characterization and experimental procedures are outlined.
- Chapter four presents and discusses the outcome of experimental works, such as product distribution, catalyst characterization, catalytic performance, reusability studies and kinetic studies.
- Chapter five concludes the research findings and recommends the direction for future work in catalytic fast pyrolysis.

## **CHAPTER TWO**

### **LITERATURE REVIEW**

#### **2.1 Introduction**

Chapter two presents a review on previous pyrolysis studies of lignocellulosic biomass. Major components in lignocellulosic biomass are described and the information on biomass selected in this study is provided. A brief review on fast pyrolysis is provided. The catalysts used in previous catalytic pyrolysis are reported, which are divided into aluminosilicate catalysts and metal-impregnated catalysts. The effects of different catalysts such as textural properties and acidity on product yield and distribution are justified. The effects of reaction parameters such as particle size, pyrolysis temperature, catalytic temperature, catalyst loading, and catalyst deactivation and reusability are studied. Lastly, the kinetic studies of biomass decomposition by Coats-Redfern calculation are reviewed, followed by a short summary for this chapter.

#### **2.2 Lignocellulosic biomass**

The utilization of biomass as energy and chemical feedstock has been studied extensively in the past few decades (Demirbaş, 2001; Börjesson et al., 2017). Biomass is a renewable resource and it provides net zero carbon dioxide production during the heat and energy production. There are different classes of biomass being used in the biomass conversion studies, such as woody biomass, aquatic biomass, herbaceous biomass and animal waste. Lignocellulosic biomass is one of the most abundant biomass that is mainly composed of cellulose, hemicellulose, lignin, and small amount of extractives and inorganic minerals. The composition of biomass

components is one of the major concerns as the three major components will give different products after decomposition (Figure 2.1).

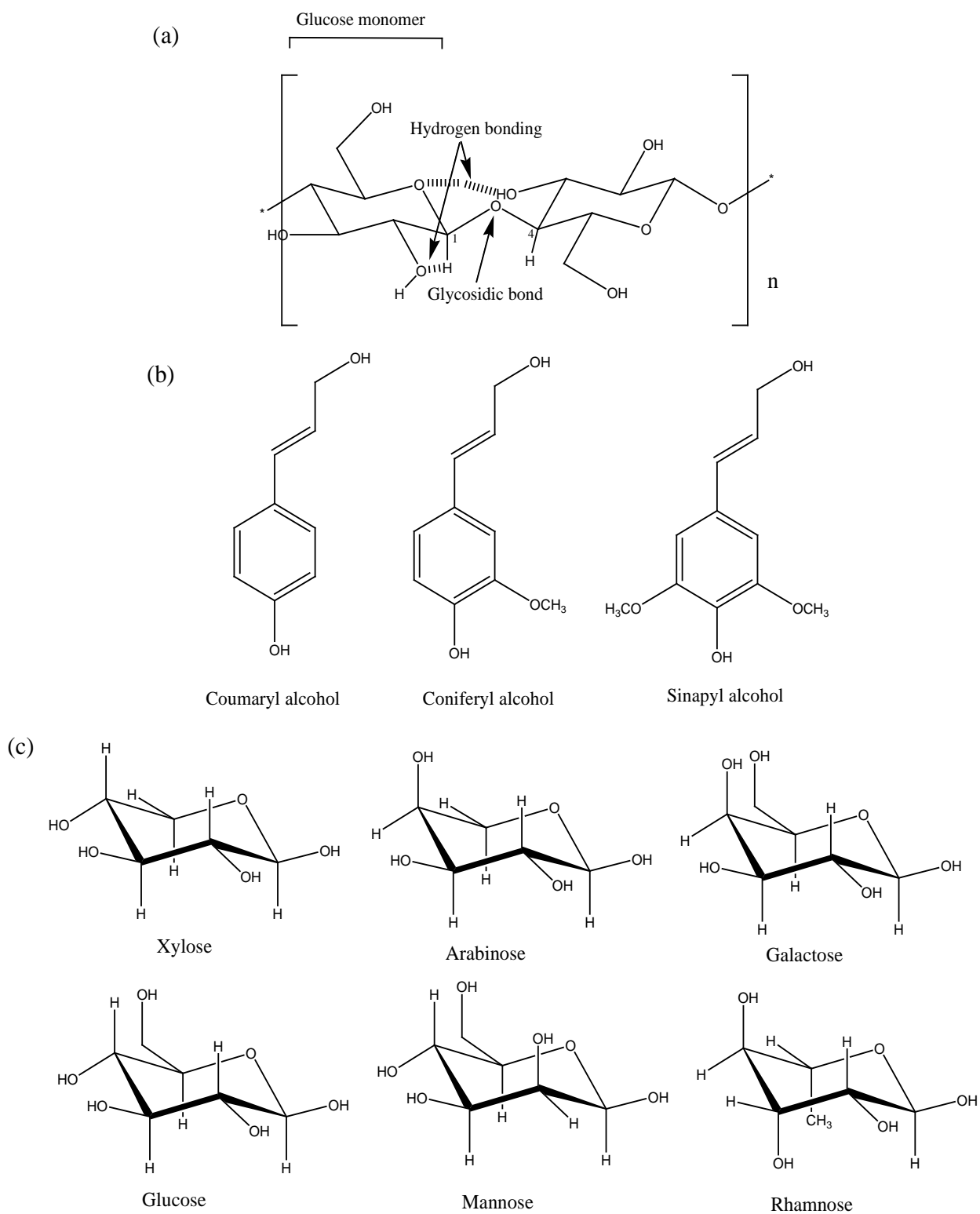


Figure 2.1 Monomer units of (a) cellulose, (b) lignin and (c) hemicellulose (Hansen and Plackett, 2008; Shahzadi et al., 2014).

Cellulose is a biopolymer composed of cellobiose linked by repeating  $\beta$ -1,4-glycosidic linkage and hydrogen bonding. It has high degree of polymerization (up to 10000) with simple and ordered structure and therefore it is thermally stable. Hemicellulose is a heteropolysaccharide composed of pentose sugars (xylose and arabinose), hexose sugars (glucose, galactose and mannose), hexuronic acids (glucuronic acid and galacturonic acid), acetyl groups, and the small quantity of rhamnose and fucose (hexose deoxy sugar) (Zhou et al., 2017). The composition of hemicellulose in different plant varies but Anca-Couce (2016) suggested that hemicellulose in hardwood contains more pentose sugars while softwood has more hexose sugars. Lignin is a randomly linked and amorphous polymer consisted of methoxylated phenylpropane (C9) structures, such as coumaryl alcohol, sinapyl alcohol and coniferyl alcohol. It has polydispersity property and its composition is different in the plants.

Lignocellulosic biomass includes a wide range of materials such as grasses or herbaceous feedstock (e.g. grass, grass silage), residues from arable land (e.g. agricultural crops and agricultural by-products), forestry residues (e.g. sawdust and residues after forest thinning), and other wastes (e.g. municipal and industrial waste) (Singh et al, 2010).

### **2.3 Fast pyrolysis**

Fast pyrolysis is a complex process that involves mass and heat transfer phenomena with different chemical reactions that can be classified into three groups: biomass devolatilization, secondary gas phase reactions, and heterogeneous reactions between solid and gas (Dupont et al., 2009). It involves rapid reaction complexes consisted of radical formation and recombination reactions, polymerization-

condensation reactions, hydrogen addition reactions, and dehydration reactions among others. The competition between repolymerization and depolymerization reactions affects the product yield distribution and the chemical distribution in bio-oil produced. Longer vapour residence time in slow pyrolysis favoured the production of bio-char or gas because of secondary repolymerization or cracking reactions promoted by the product char. Table 2.1 summarizes the product yield distribution in fast pyrolysis of lignocellulosic biomass while Figure 2.2 shows the main reactions in pyrolysis.

Table 2.1 Summary of product yield distribution in fast pyrolysis of lignocellulosic biomass.

Feedstock	Product yield (wt%, dry basis)			Ref.
	Solid	Liquid	Gas	
Cellulose*	21	69	10	(Stefanidis et al., 2014)
Xylan*	34	44	22	(Stefanidis et al., 2014)
Lignin*	48	43	9	(Stefanidis et al., 2014)
Peanut shell	32-48	11-22	36-56	(Yuan et al., 2015)
Pine needle	30-52	15-22	30-52	(Yuan et al., 2015)
Corn cob	48-64	8-15	23-42	(Yuan et al., 2015)
Red oak	18-58	28-62	11-22	(Gable and Brown, 2016)
Cotton stalk	29	50	21	(Chen et al., 2017a)
Beech wood	10.3-40.6	34.8-62.4	6.1-51.5	(Guizani et al., 2017)
Sugarcane bagasse	25-30	38-51	11-22	(Al Arni, 2018)
Sunflower seed hull	27	45	28	(Casoni et al., 2018)
Empty fruit bunch	30-31	41-45	26-29	(Ro et al., 2018)

\* Commercial source

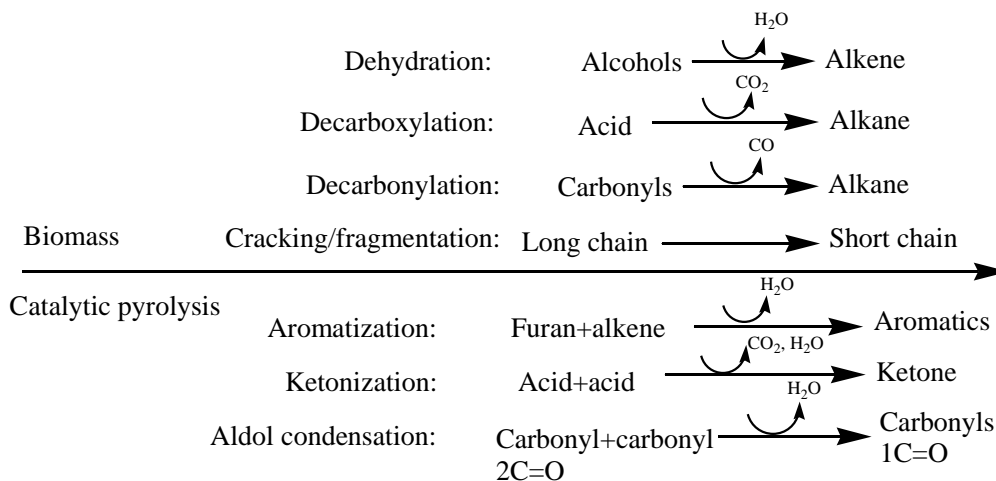


Figure 2.2 The main reactions in fast pyrolysis mechanism (Wang et al., 2017a).

Due to these complex reactions, bio-oil might consist of more than 300 organic compounds (Bulushev and Ross, 2011). In general, the major products from decomposition of cellulose and hemicellulose are mainly oxygenated compounds such as sugar derivatives, furans and miscellaneous oxygenates. These oxygenates are usually converted into smaller oxygenated compounds such as acids, alcohol, esters and carbonyls through secondary reactions. For the lignin decomposition, aromatic compounds such as phenols, guaiacols and syringols are the main products (Huber et al., 2006). Table 2.2 summarizes the composition and yield of bio-oil.

Table 2.2 Chemical compositions of bio-oil (Huber et al., 2006).

No.	Chemicals	Yield (wt%)	Examples
1.	Acids	2-26	Formic acid, acetic acid, propanoic acid
2.	Esters	0-3	Methyl formate, butyrolactone, angelicalactone
3.	Alcohols	2-6	Methanol, ethanol, ethylene glycol
4.	Ketones	4-6	Acetone
5.	Aldehydes	2-20	Formaldehyde, acetaldehyde, ethanedial
6.	Misc oxy	4-26	Glycolaldehyde, acetal
7.	Sugars	5-13	Anhydroglucose, glucose, fructose
8.	Furans	1-11	Furfural, 5-hydroxymethylfurfural
9.	Phenols	2-12	Phenol, dihydroxybenzene, dimethylphenol
10.	Guaiacols	2-15	Isoeugenol, eugenol, methyl guaiacol
11.	Syringols	1-10	Syringols



Azeez et al. (2010) reported the product yield and chemical distribution in bio-oil produced from fast pyrolysis of five plant-based feedstocks. Samples with high amount of volatile matters give high liquid product with major oxygenated products such as acetic acid and hydroxyacetaldehyde. Feedstock with higher lignin content tends to produce liquid product with high organic yield of hydroxyacetaldehyde and levoglucosan. The ash content affects the cracking and repolymerization reactions during the decomposition process. Thus, high char yield and liquid yield with high aqueous content were obtained. The heating values of all the bio-oils were significantly higher than that of feedstock, showing the fast pyrolysis is effective in biomass conversion.

Stefanidis et al. (2014) provided in-depth analysis of the fast pyrolysis study of biomass components, which are cellulose, hemicellulose and lignin. Cellulose gave bio-oil with low water content and high organic contents. The major chemicals were levoglucosan, simple phenols, carbonyls and alcohols. Xylan (commercial type of hemicellulose) produced high yield of gaseous products and bio-oil with high water content and low organic content due to its high ash content that enhanced cracking of heavy molecules. The bio-oil contains ketones (mainly hydroxyacetone) and phenolic compounds (such as simple phenols and methyl-substituted phenols). Char was the primary product in fast pyrolysis of lignin followed by bio-oil and gas. Phenolic compounds were the major chemicals in bio-oil due to its C9 structure.

Zhang et al. (2017b) investigated the properties of bio-oil produced from fast pyrolysis of corn stalk residue (CSR) and cassava rhizome residue (CRR). CSR is a lignin-rich biomass while CRR contains higher amount of holocellulose (cellulose and hemicellulose). Thus, CSR gave higher char yield and CRR gave higher liquid yield. The bio-oil of CSR contains mainly carboxylic acid, phenolic compounds and

furan derivatives while the bio-oil of CRR contains carboxylic acid, furan derivatives, alcohol, ketone and aromatic compounds. This showed that the difference in biomass component did affect the composition of bio-oil produced.

Crude bio-oil can be used as a fuel additive for some boilers and engines. It had been fired in a diesel test engines with limited operation time (Kan et al., 2016). However, catalytic upgrading of bio-oil must be done to overcome the weaknesses of crude bio-oil such as high water and oxygen content, corrosive, poor volatility, too viscous and cause coking. For the use of bio-oil in chemical production, further upgrading also has to be done to enhance the product selectivity.

## **2.4 Catalytic fast pyrolysis**

In the past two decades, bio-oil upgrading has been one of the major interesting research subjects due to the potential of bio-oil to be used as renewable fuel and chemical intermediate. It has the advantages over raw biomass such as cleaner (less impurities), easier to transport and higher energy content. There are many weaknesses of the bio-oil properties that need to be addressed. Bio-oil without further upgrading cannot be used directly in any application due to its high oxygenates and water content. This crude bio-oil is unstable, highly corrosive and immiscible with petrol and diesel. It also contains long carbon chain (up to 100), where the gasoline and diesel have much shorter chain lengths (gasoline: C<sub>5</sub>-C<sub>10</sub>; diesel: C<sub>12</sub>-C<sub>20</sub>). Thus, bio-oil upgrading means to minimize the undesirable properties.

One of the most significant current discussions in bio-oil upgrading is heterogeneous catalysis. The heterogeneous catalytic pyrolysis can be done in in-situ and ex-situ methods. In-situ method involves the direct contact of catalyst and

biomass feedstock while *ex-situ* method involves the contact of liquid bio-oil or pyrolytic vapour with catalyst (Kabir and Hameed, 2017). The ideal catalyst for bio-oil upgrading should be able to enhance the quality and yield of bio-oil, reduce the oxygen content (ideally by decarboxylation to avoid diminishing of hydrogen content), reduce undesired compounds, and has good resistance towards thermal deactivation (Lappas et al., 2012).

The major catalytic reaction involved in catalytic pyrolysis is fragmentation reactions. Fragmentation or cracking reaction is a complex reaction that involves C-C bond cleavage, hydrogen transfer, isomerization, aromatic side chain scission and deoxygenation reactions (Zhang et al., 2013). Dehydration, decarboxylation, decarbonylation and demethoxylation are the common deoxygenation reactions that remove oxygen in the form of water, carbon dioxide, carbon monoxide and methanol, respectively (Wang et al., 2017a). Thus, the pyrolysis mechanism can be predicted through the composition of non-condensable gas. The target products for catalytic cracking are straight chain hydrocarbon and monoaromatic compounds with high heating values. Table 2.3 shows the reaction mechanisms involved in catalytic upgrading process.

A considerable amount of literature has been published on the application of different catalysts in catalytic pyrolysis (Stöcker, 2008; Lappas et al., 2012; Liu et al., 2014; Kabir and Hameed, 2017). The catalyst development is complicated as the formation and properties of catalyst have to be considered, such as tailoring the particle size, porosity, acid-base properties, reusability and the interaction between incorporated and support materials. Desired catalyst should exhibit good selectivity on desired products, good stability over cycle reactions, and good accessibility of reactants and products to active sites. Thus, it is important to understand the reaction

mechanisms, desired products and behaviour of catalyst chosen in order to optimize the product yield and selectivity. This section discussed two classes of catalysts used in bio-oil upgrading, which are acidic catalysts and metal-impregnated catalysts.

Table 2.3 Reaction mechanisms in catalytic pyrolysis (Liu et al., 2014).

Reaction	Reactants	Target products	Catalyst
Cracking (Dehydration, decarboxylation, decarbonylation)	1. Unstable oxygenates (acetic acid, propanoic acid, cyclopentanone, alcohol)	C <sub>1</sub> -C <sub>4</sub> hydrocarbons	Solid acids, metal oxides, inorganic salts
	2. Thermally stable oxygenates (sorbitol, glycerol)	Olefins, aromatics, light paraffin	
	3. Benzenediol/benzenetriol	Phenol	
	4. Guaiacol	1,2-dihydroxybenzene, methane, o-cresol, 2-hydroxybenzaldehyde, coke	
Aromatization	Small oxygenates (acids, esters, ethers, alcohols, ketones) and olefins	Aromatic hydrocarbons	HZSM-5
Ketonization/ aldol condensation	Carboxylic acids, esters	Ketone or aldehyde (longer chain intermediates to convert into gasoline)	Solid oxide, Brønsted and Lewis acid
Hydro-deoxygenation	Phenolics compounds (guaiacol, catechol, anisole), carbonyl compounds (aldehyde, carboxylic acids)	Phenol, aldehyde, alcohol	Noble metal
Steam reforming	Small oxygenates (acids, esters, ethers, alcohols, ketones)	H <sub>2</sub>	Ni-based, Co-based

In order to select suitable catalyst for catalytic fast pyrolysis, the textural properties and porosity of the catalyst should be concerned. Zeolites such as HZSM-5 and ZSM-5 are the mostly commonly used catalyst in catalytic fast pyrolysis. However, the microporous characteristic of these catalysts leads to rapid catalyst deactivation by coke formation. Liu et al. (2014) summarized that zeolites with medium pore size, moderate pore volume and steric hindrance are suitable for the production of aromatic compounds. In context of physisorption, the pores can be classified into micropores (pore width <2 nm), mesopores (pore width 2 nm to 50 nm) and macropores (pore width exceed 50 nm).

At year 1985, six types of physisorption isotherms and four types of hysteresis loops were recommended by IUPAC and it had been refined in the IUPAC technical report written by Thommes et al. (2015). The proposed updated adsorption isotherms and hysteresis loops were shown in Figure 2.3 and Figure 2.4. Type I(a) isotherm is given to microporous material with mainly micropores with pore width less than 1 nm while Type I(b) isotherm is found in microporous material with wider pore width and possibly narrow mesopores (pore width up to 2.5 nm). Type II and III isotherms are given to the nonporous or macroporous materials where the high position of point B found in Type II isotherm indicates the presence of micropores. Type IV isotherms are given to the mesoporous materials while the presence of hysteresis loop in Type IV(a) isotherm occurs when the pore width exceeds a certain critical width (pore width wider than 4 nm) and Type IV(b) isotherm is found in the mesoporous material with smaller pore width. Type V isotherm is similar to Type III isotherm due to the weak adsorbent-adsorbate interaction and usually observed in water adsorption of hydrophobic microporous and mesoporous adsorbent. Type VI

isotherm represents the layer-layer adsorption on a highly uniform non-porous surface, such as graphite.

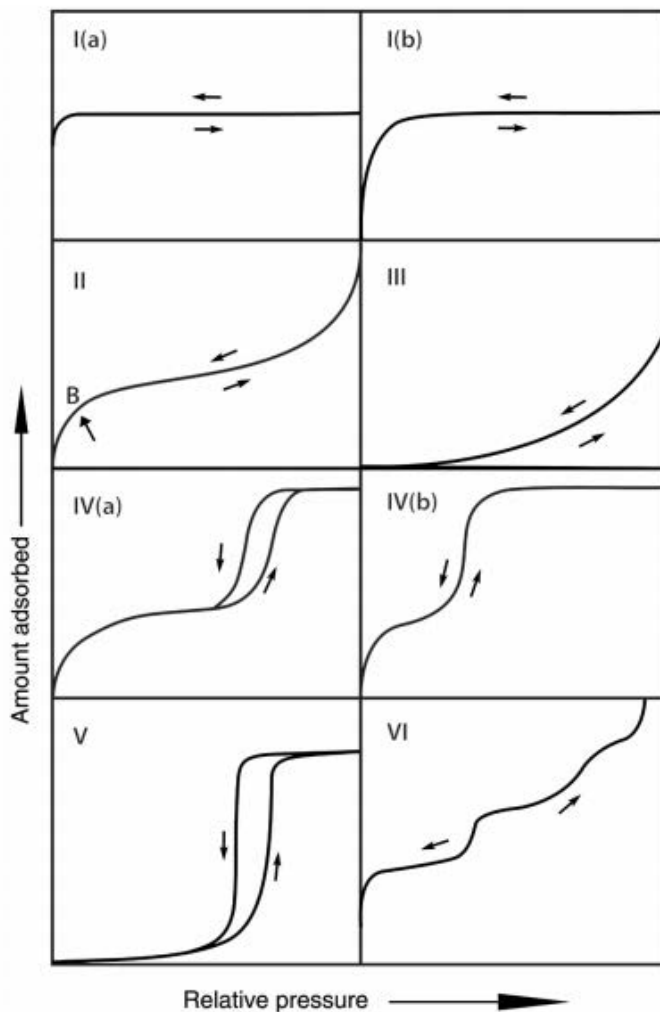


Figure 2.3 Classification of physisorption isotherms (Thommes et al., 2015).

The hysteresis loop is generated associated with capillary condensation and the forms of hysteresis loop can be affected by the adsorption metastability and/or network effects. H1 hysteresis loop is found in material with narrow range of uniform mesopores. H2 hysteresis loop can be attributed to the pore blocking or percolation where the size distribution of neck width for H2(b) hysteresis loop is larger than that of H2(a) hysteresis loop. H3 hysteresis loop is given to non-rigid aggregates of plate-like particles or macroporous material which is not completely

filled with pore condensate, H4 hysteresis loop is found in material containing micropores such as zeolites and carbons, while H5 hysteresis loop is associated with partially blocked mesopores.

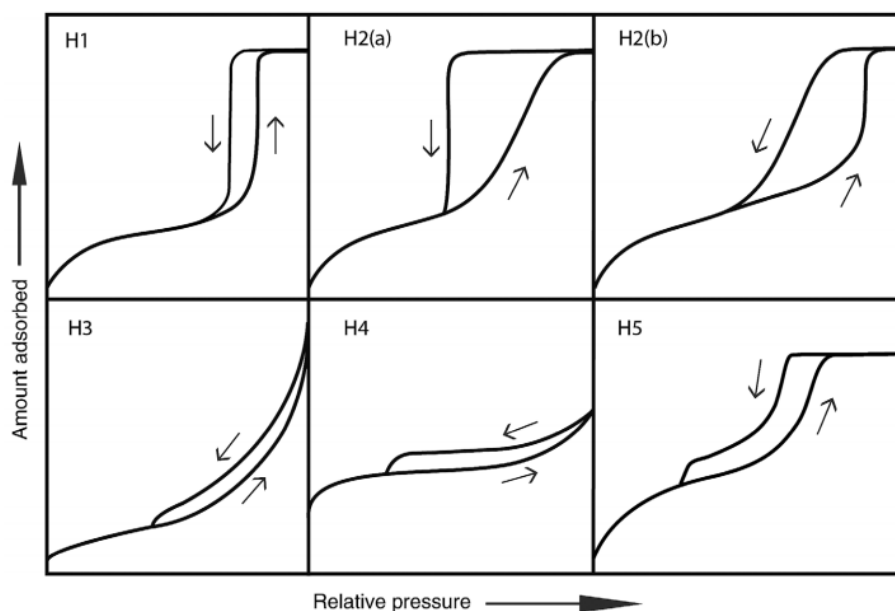


Figure 2.4 Classification of hysteresis loops (Thommes et al., 2015).

### 2.4.1 Acid catalysts

Acid catalysts are the major heterogeneous catalyst used in catalytic upgrading of bio-oil, which can be classified into Lewis-type (electron acceptor), Brønsted-type (proton donor), and combined properties. Both Lewis and Brønsted acid sites can enhance the depolymerization of cellulose and also the secondary cracking of primary vapour. Homogeneous Brønsted acids such as sulphuric acid and phosphoric acid were used to hydrolyze pentosan into pentose that can be further dehydrated into furfural (Agirrezabal-Telleria et al., 2011). Vitolo et al. (2001) proposed that the major active sites used in catalytic pyrolysis were Brønsted acid sites that function through a carbonium ion mechanism to promote the catalytic reactions. Even Lewis acid catalysts such as  $ZnCl_2$  and  $Fe_2(SO_4)_3$  had been used in

the furfural production from biomass catalytic pyrolysis and it showed that furfural was one of the major products in catalytic pyrolysis (Oh et al., 2013), the role of Lewis acid in the mechanism is not clear and established as Brønsted acid.

In general, acidic metal oxides can enhance the deoxygenation reaction, especially dehydration and decarbonylation, thus reduce the oxygen content in bio-oil (Wang et al., 2017a). Besides that, it also promotes the cracking of large molecules into smaller products. The most common acidic metal oxide used in catalytic pyrolysis is aluminosilicate. Amorphous aluminosilicate is a complex system with unique acidic characteristics which are halfway between those of alumina and zeolites. The silicon and aluminium atoms distribution on catalyst depends on the synthesis methods, which are the direct synthesis and impregnation methods. Higher aluminum content or lower silica-to-alumina ratio usually leads to higher acid sites concentration, especially for Brønsted acid sites that formed through the bridged hydroxyl group formation between aluminium and silicon atoms (Leydier et al., 2011). In catalytic pyrolysis, mesoporous aluminosilicate may be preferred over zeolites due to their larger pore size which facilitates reactants and products diffusion. Besides that, amorphous aluminosilicate has milder acidity than zeolites and this enhances the cracking selectivity (Mardkhe et al., 2014).

The effects of amorphous silica-alumina on product yield and composition are different from alumina. Triantafyllidis et al. (2007) synthesized two types of aluminosilicates (hexagonal and wormhole type) from zeolite Beta by hydrothermal method. The bio-oil yield decreased while coke formation increased in the presence of catalyst. Hexagonal type aluminosilicate decreased gas formation as decarbonylation and decarboxylation reactions were reduced. Wormhole type aluminosilicate has higher acidity and larger pore size, and this catalyst enhanced gas